PHILOSOPHICAL TRANSACTIONS A

royalsocietypublishing.org/journal/rsta

Review

Check for updates

Cite this article: Segall P. 2019 Magma chambers: what we can, and cannot, learn from volcano geodesy. *Phil. Trans. R. Soc. A* **377**: 20180158.
http://dx.doi.org/10.1098/rsta.2018.0158

Accepted: 11 August 2018

One contribution of 15 to a Theo Murphy meeting issue 'Magma reservoir architecture and dynamics'.

Subject Areas:
volcanology, geophysics

Keywords:
volcano geodesy, volcano deformation, magma recharge, viscoelasticity, rheology

Author for correspondence:
Paul Segall
e-mail: segall@stanford.edu

THE ROYAL SOCIETY
PUBLISHING

Magma chambers: what we can, and cannot, learn from volcano geodesy

Paul Segall

Geophysics Department, Stanford University, Stanford, CA 94305-2215, USA

PS, 0000-0001-5973-471X

Geodetic observations on volcanoes can reveal important aspects of crustal magma chambers. The rate of decay of deformation with distance reflects the centroid depth of the chamber. The amplitude of the deformation is proportional to the product of the pressure change and volume of the reservoir. The ratio of horizontal to vertical displacement is sensitive to chamber shape: sills are efficient at generating vertical displacement, while stocks produce more horizontal deformation. Geodesy alone cannot constrain important parameters such as chamber volume or pressure; furthermore, kinematic models have no predictive power. Elastic response combined with influx proportional to pressure gradient predicts an exponentially decaying flux, leading to saw-tooth inflation cycles observed at some volcanoes. Yet many magmatic systems exhibit more complex temporal behaviour. Wall rock adjacent to magma reservoirs cannot behave fully elastically. Modern conceptual models of magma chambers also include cumulate and/or mush zones, with potentially multi-level melt lenses. A viscoelastic shell surrounding a spherical magma chamber significantly modifies the predicted time-dependent response; post-eruptive inflation can occur without recharge if the magma is sufficiently incompressible relative to the surrounding crust (Segall P. 2016 *J. Geophys. Res. Solid Earth*, **121**, 8501–8522). Numerical calculations confirm this behaviour for both oblate and prolate ellipsoidal chambers surrounded by viscoelastic aureoles. Interestingly, the response to a nearly instantaneous pressure drop during an explosive eruption can be non-monotonic as the rock around the chamber relaxes at different rates. Pressure-dependent recharge of a non-Newtonian magma in an elastic crust leads to an initially high rate of inflation which slows over time; behaviour that has been observed in some magmatic systems. I close by discussing future challenges in volcano geodesy.

This article is part of the Theo Murphy meeting issue 'Magma reservoir architecture and dynamics'.

royalsocietypublishing.org/journal/rsta *Phil. Trans. R. Soc. A* **377**: 20180158

1. Introduction

Measurements at many volcanoes show that they *inflate* as magma accumulates in crustal reservoirs, and then *deflate* as magma is withdrawn, due to either eruption or intrusion. The association is so strong that uplift is nearly universally associated with magma accumulation, e.g. 'Swelling of a volcano signals that magma has accumulated near the surface'[1]. Inflation is thus taken as a possible indicator of an impending eruption. Nevertheless, it should be noted that some eruptions occur without measurable inflation, and some volcanoes inflate without erupting (e.g. [1]); the latter is particularly notable at restless silicic calderas.

Volcano deformation has traditionally been interpreted in terms of simplified chamber geometries, such as spheres, ellipsoids or penny-shaped cracks embedded in elastic half-spaces. In most cases, the walls of the magma bodies are subject to uniform pressure and vanishing shear stress. For example, displacements on the Earth's surface resulting from a pressure change Δp in a spherical magma chamber, in the limit that the magma chamber depth d is substantially larger than its radius, is

$$u_i(r,t) = \frac{3(1-\nu)}{4\pi}\,\frac{\Delta p(t)V_0}{\mu d^2}\,\frac{\xi_i}{[(r/d)^2+1]^{3/2}}, \tag{1.1}$$

where r is the radial distance from the source on the Earth's surface, V_0 is the volume of the magma chamber, d is the depth to the chamber centroid, and μ and ν are shear modulus and Poisson's ratio. In (1.1), $\xi_z = 1$ for vertical displacement, while for radial displacement $\xi_r = r/d$. This is the celebrated Mogi model [2], although this study built on prior work of Sezawa & Yamakawa (see Origins in [3] for perspective).

From the rate at which the displacement decays with distance, one can determine the source depth d (figure 1). On the other hand, the magnitude of the displacement scales with the product $\Delta p V_0$ so that it is not possible to independently determine either the chamber volume or the pressure change. Higher-order approximations can potentially separate pressure change and volume [4]; however in practice this has not proven practicable. Note, however, that the volume change (during the period over which the displacements u_i occur) can be estimated from $\Delta V = 3\Delta p V_0/4\mu$.

Comparable analytical and semi-analytical models have been developed for ellipsoidal chambers [5,6] and penny-shaped sills [7]. These show that prolate ellipsoids are relatively efficient at generating horizontal displacements relative to the vertical, while sills and oblate ellipsoids are efficient at generating vertical displacement (figure 1). In summary, geodetic data generally provide: (i) some information on the source depth and horizontal location (from the position of peak uplift), (ii) some constraint on source shape, from the ratio of vertical to horizontal deformation, and (iii) some measure of source strength, proportional to $\Delta p V_0$ (e.g. [3,8]). It should be noted that sub-vertical dykes have very distinctive deformation patterns and are relatively easily identified. Of course, these model geometries are highly idealized relative to what one observes in eroded magma reservoirs.

Traditional geodetic approaches cannot resolve the total magma chamber volume V_0, the pressure acting on the chamber, or much about the properties of the fluid within the chamber. It is true that simultaneous measurements of deformation and microgravity change have the potential to place constraints on the density of the fluid phase (e.g. [9–11]). Essentially, the deformation resolves ΔV, while gravity change constrains the increment in mass. In practice, however, it

[1]https://en.wikipedia.org/wiki/Prediction_of_volcanic_activity#Ground_deformation.

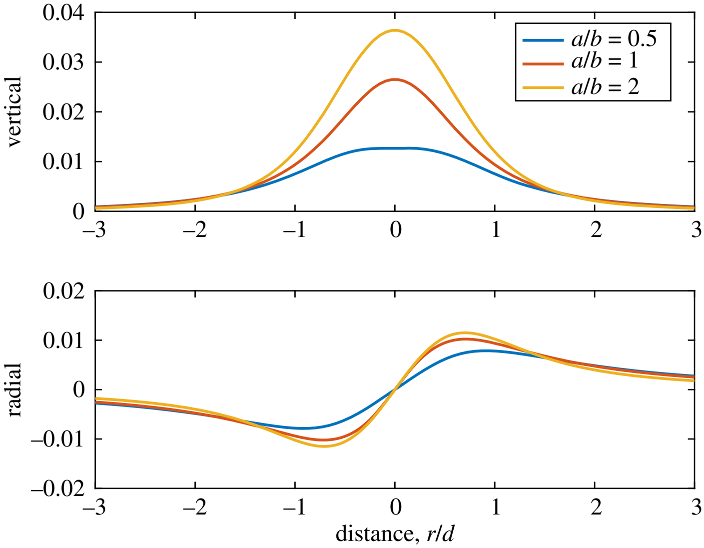

Figure 1. Vertical and radial displacements from ellipsoidal magma chambers. Here a/b is ratio of horizontal to vertical semi-axes; $a/b = 1$ corresponding to the spherical Mogi geometry. The y-axis is normalized such that $\Delta V/d^2 = 1/9$. Calculations based on expressions and code from Cervelli [6].

can be challenging to remove environmental mass changes, notably groundwater in unconfined aquifers, and one must also account for changes in gravity due to deformation in addition to the increase (or decrease) of fluid mass (see [3] ch. 9).

Finally, it must be noted that kinematic models have no predictive power, in that they are not representing evolving physical systems. That is not to say that patterns of behaviour cannot be used in empirical forecasts; for example, shallowing of deformation might be taken as precursory to an eruption.

Elastic half-space models are certainly highly idealized relative to the Earth. Considerable research has been undertaken to include the effects of elastic heterogeneity and realistic topography (e.g. [12–14]). In addition, for some time it has been recognized that the solid crust immediately adjacent to a magma chamber cannot deform in a purely elastic fashion due to the high temperatures expected there; rather the adjacent materials are more likely to respond in a viscoelastic manner. Furthermore, conceptual models of magma chambers often include significant zones of cumulates or partially crystalline mush within the chamber, as illustrated in figure 2. Section 2 describes simple models with viscoelastic aureoles surrounding the fluid magma reservoir.

(a) Time-dependent recharge

Simple models of melt recharge from depth provide a reasonable approximation to time-dependent re-pressurization of elastic magma chambers. Conservation of mass of magma m in the reservoir requires

$$\frac{\mathrm{d}m}{\mathrm{d}t} = \frac{\mathrm{d}(\rho V)}{\mathrm{d}t} = \rho V_0(\beta_\mathrm{m} + \beta_\mathrm{c})\frac{\mathrm{d}p}{\mathrm{d}t} = q_\mathrm{in} - q_\mathrm{out}, \tag{1.2}$$

where ρ is the magma density in the initial state, V_0 is the initial magma chamber volume, β_m is the magma compressibility, $\beta_\mathrm{c} = (1/V)\partial V/\partial p$ is the *chamber compressibility* and q are mass flow rates. For a spherical chamber far from the free surface relative to its radius, $\beta_\mathrm{c} = \frac{3}{4}\mu$, where μ is the shear modulus. Following an eruption, there is no outflow, $q_\mathrm{out} = 0$. A first-order approximation takes the flux into the chamber to be proportional to the pressure difference, $q_\mathrm{in} = \Omega(p^\infty - p)$, where p^∞ is the pressure of a deep (possibly mantle) reservoir assumed to

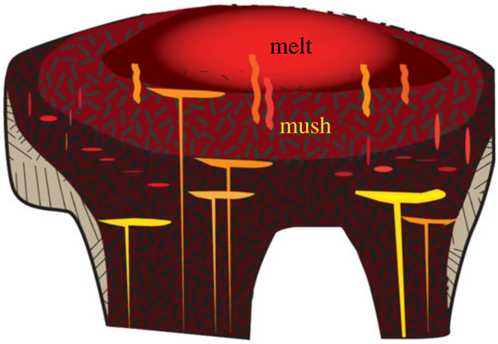

Figure 2. Conceptual model of a silicic magma reservoir which is supplied with more mafic melts from below. From Cashman *et al.* [15].

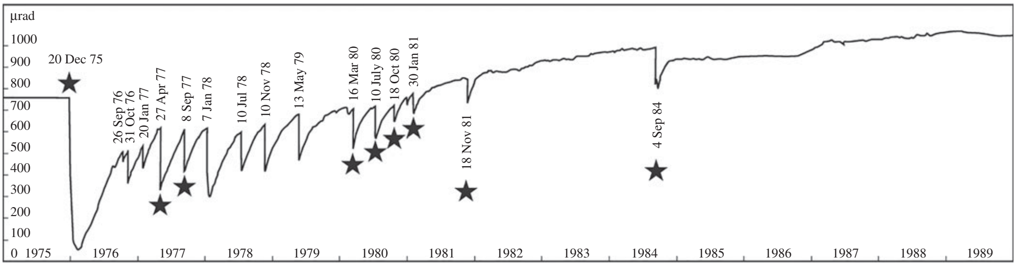

Figure 3. Water tube tilt record at Krafla power plant. Positive tilt is inflation; the sudden drops are either intrusions into the adjacent rift zone or eruptions (stars). After Sturkell *et al.* [17].

be maintained constant, and Ω is a conductivity parameter with units $\mathrm{kg\,Pa^{-1}\,s^{-1}}$ (e.g. [16]). Combining,

$$p^{\infty} - p(t) = \tau \frac{\mathrm{d}p}{\mathrm{d}t} \quad \text{with } \tau \equiv \frac{\rho V_0(\beta_{\mathrm{m}} + \beta_{\mathrm{c}})}{\Omega}, \tag{1.3}$$

which has the solution

$$p(t) = [p^{\infty} - (p^{\infty} - p_0)]\mathrm{e}^{-t/\tau}. \tag{1.4}$$

This characteristic saw-tooth-like re-pressurization is exhibited in several long-term records at frequently erupting basaltic shield volcanoes, including at Kilauea during the early phases of the Pu'u O'o eruption, and at Krafla in Iceland, where a sequence of tilt cycles were associated with eruptions and intrusions during the fissure swarms of the late 1970s and early 1980s (figure 3). In the latter example, the characteristic time τ appears to be of the order of months.

2. Review of viscoelastic effects

The effects of viscoelastic relaxation on observable deformation have been considered by a number of authors. Dragoni & Magnanensi [18] derived an analytical result for a spherical chamber surrounded by a spherical viscoelastic shell; these results formed the basis of the work in Segall [19] described below. Bonafede *et al.* [20] found solutions for point sources in a viscoelastic half-space. Newman *et al.* [21,22] applied the analytical model of Dragoni & Magnanensi [18], and finite-element method (FEM) calculations, respectively, to model time-dependent deformation in Long Valley Caldera. Del Negro *et al.* [23] and Masterlark *et al.* [24] applied steady-state thermal models and temperature-dependent rheology to FEM modelling of Etna and Okmok volcano, respectively. Yamasaki *et al.* [25] modelled deformation resulting from sill intrusion in an elastic upper crust overlying a Maxwell viscoelastic lower crust and mantle, while Currenti [26] explores surface deformation and gravity change due to ellipsoidal magma chambers in viscoelastic media.

Some insight into the challenges that viscoelastic effects pose can be gained by considering the response of time-varying pressure change in a spherical magma chamber (with radius R_1) surrounded by a spherical shell (radius R_2) with Maxwell rheology, following Dragoni & Magnanensi [18]. In this case, the displacements on the surface of the elastic region can be (approximately) written as a function of radial distance r, and time t,

$$u_i(r,t) = \frac{3(1-\nu)}{4\pi}\frac{V_0}{\mu d^2}\left[\frac{\xi_i}{(1+\zeta^2)^{3/2}}\right]\left\{\delta p_0^+ f(t/t_\mathrm{R}) + \int_0^t \frac{\mathrm{d}p(t')}{\mathrm{d}t'} g\left(\frac{t-t'}{t_\mathrm{R}}\right)\mathrm{d}t'\right\}. \tag{2.1}$$

The term in braces is the pressure change; the geometric dependence is the same as in the Mogi solution, where $\zeta = r/d$ and ξ_i is the same as in equation (1.1). Here δp_0^+ is the pressure change at $t = 0^+$, and $f(t/t_\mathrm{R})$ and $g((t-t')/t_\mathrm{R})$ are dimensionless functions that depend on the relaxation time, t_R, which is given by

$$t_\mathrm{R} = \frac{3\eta(1-\nu)}{\mu(1+\nu)}\left(\frac{R_2}{R_1}\right)^3, \tag{2.2}$$

where η is the viscosity of the shell. For this geometry, the relaxation time depends on the ratio of the radii cubed as well as the intrinsic Maxwell time η/μ [18]. Equation (2.1) involves a convolution of the pressure rate history with the relaxation function $g((t-t')/t_\mathrm{R})$. Solving (2.1) for the pressure rate history from observed displacements is thus a deconvolution. The difficulty is that, without knowing the relaxation time (that is, viscosity), one cannot do the deconvolution to solve for the pressure history. The challenge in constraining wall rock viscosity is that it depends not only on lithology and temperature but also on grain size (for diffusion creep) and concentration of intra-crystalline water within the dominant silicate phases. For reference, viscosities ranging from 10^{15} to 10^{19} Pa s, and standard crustal shear moduli (3×10^{10} Pa) lead to characteristic times of from 10^{-3} to 10 years.

Some progress can be made by considering the response to a sudden pressure drop during an explosive eruption (figure 4), which basically yields the impulse response of the crust. I previously argued [19] that two things can happen following the pressure drop: First, the sudden change in pressure will initiate a viscoelastic response of the crust surrounding the chamber. Secondly, the reduced pressure within the magma chamber will tend to drive increased flux into the chamber from below.

The model is illustrated in figure 4. The magma chamber is fed by a deep source that is assumed to be sustained at constant pressure. Pressure p^∞ is the chamber pressure in magma-static equilibrium with the source region, i.e. $p_\mathrm{deep} = p^\infty + \rho g H$, where H is the vertical distance between the top of the source region and the chamber centroid. Prior to the eruption, the magma chamber may be inflating such that $p(t=0^-) \equiv p_0^- \le p^\infty$.

During an eruption, mass is evacuated from the chamber (assumed instantaneously) such that the pressure drops to $p_0^- + \delta p(t=0^+) \equiv p_0^- + \delta p_0^+$, where $\delta p_0^+ < 0$. The shell surrounding the magma chamber initially responds elastically, but with time magma flows from the deep source into the chamber, and the viscoelastic shell relaxes. I assume for simplicity that mass flux into the chamber is proportional to the pressure gradient $\Omega(p^\infty - p)$ as in the analysis for the elastic system leading to equation (1.3).

Segall [19] gives an approximate analytical solution for the surface displacements u_i, due to a chamber of radius R_1 at depth d, with viscoelastic aureole of radius R_2, as

$$u_i(z=0,r,t) = \frac{3(1-\nu)}{4\pi}\frac{V_0}{\mu d^2}\left[\frac{\xi_i}{(1+\zeta^2)^{3/2}}\right]\{f_1 + f_2 e^{s_1 t} + f_3 e^{s_2 t}\}, \tag{2.3}$$

where f_j, $j = 1,2,3$, are functions of $\Delta p_0 \equiv p^\infty - p_0^-$, $(R_2/R_1)^3$, τ, t_R, s_1, s_2, δp_0^+ and given in Segall [19]. Recall that τ is the characteristic time for elastic refilling, as defined in (1.3). The reciprocal

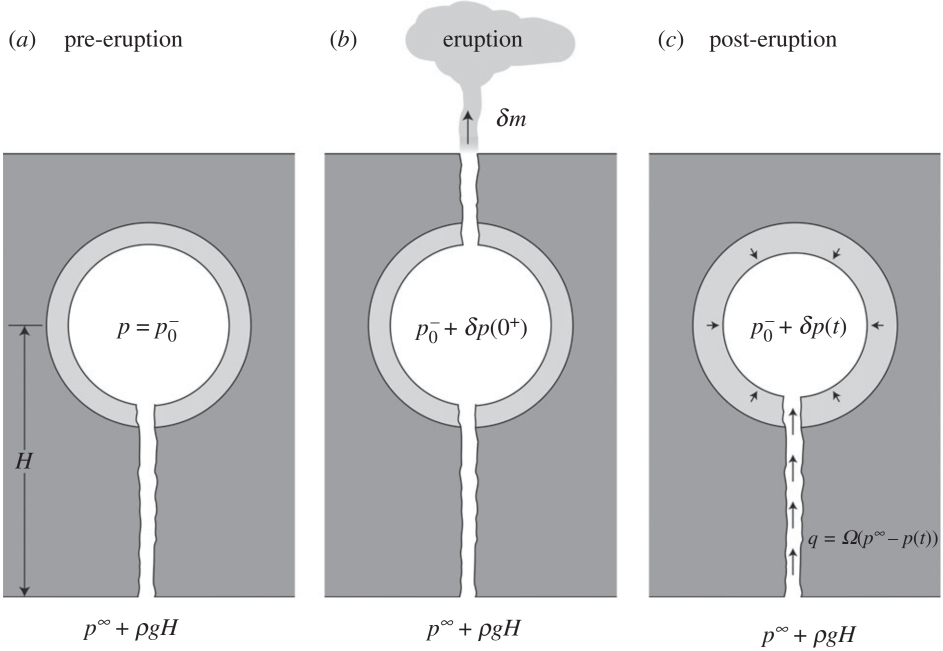

Figure 4. Schematic of magma system. (*a*) Pre-eruptive state, with magma chamber pressure p_0^- and deep reservoir at pressure $p_{\mathrm{deep}} = p^\infty + \rho g H$. (*b*) Co-eruptive state, mass δm is erupted causing the chamber pressure to drop to $p_0^- + \delta p(t = 0^+)$. The viscoelastic shell surrounding magma chamber responds elastically. (*c*) Post-eruptive state, magma flows into the chamber from deep reservoir, viscoelastic shell deforms, both contributing to a time-dependent pressure $p_0^- + \delta p(t)$. After Segall [19].

characteristic times, s_1 and s_2, are the roots of a quadratic,

$$s_{1,2} = -\frac{t_{\mathrm{R}}^{-1}(1+\mathcal{B}\alpha)+\tau^{-1}}{2} \pm \frac{1}{2}\sqrt{(t_{\mathrm{R}}^{-1}(1+\mathcal{B}\alpha)+\tau^{-1})^2 - 4\tau^{-1}t_{\mathrm{R}}^{-1}}, \tag{2.4}$$

where

$$\alpha = \frac{3(1-\nu)}{(1+\nu)}\left[\left(\frac{R_2}{R_1}\right)^3 - 1\right] \tag{2.5}$$

and

$$\mathcal{B} = \frac{\beta_{\mathrm{c}}}{\beta_{\mathrm{m}} + \beta_{\mathrm{c}}}. \tag{2.6}$$

Recall that β_{m} is the magma compressibility, while β_{c} is the chamber compressibility. Equation (2.4) reveals that the displacement history depends on the relaxation time t_{R} and the characteristic refilling time τ. In the *no-recharge* limit, the elastic refilling time is infinite, $t_{\mathrm{R}}/\tau \to 0$, and the single non-zero root in (2.4) is $-(1+\mathcal{B}\alpha)/t_{\mathrm{R}}$. In the opposite limit, the Maxwell time is infinite, $t_{\mathrm{R}}/\tau \to \infty$, and the single non-zero root in (2.4) is τ, the elastic refilling time. Other than in these limiting cases, the characteristic relaxation times in (2.3) are not equal to either t_{R} or τ.

(a) Inflation without recharge

A rather surprising result of this analysis was the recognition that the model predicts that there can be partial re-inflation following an eruption with *no recharge* into the system, if the magma is sufficiently incompressible. This contrasts with general beliefs as exemplified by the quote from

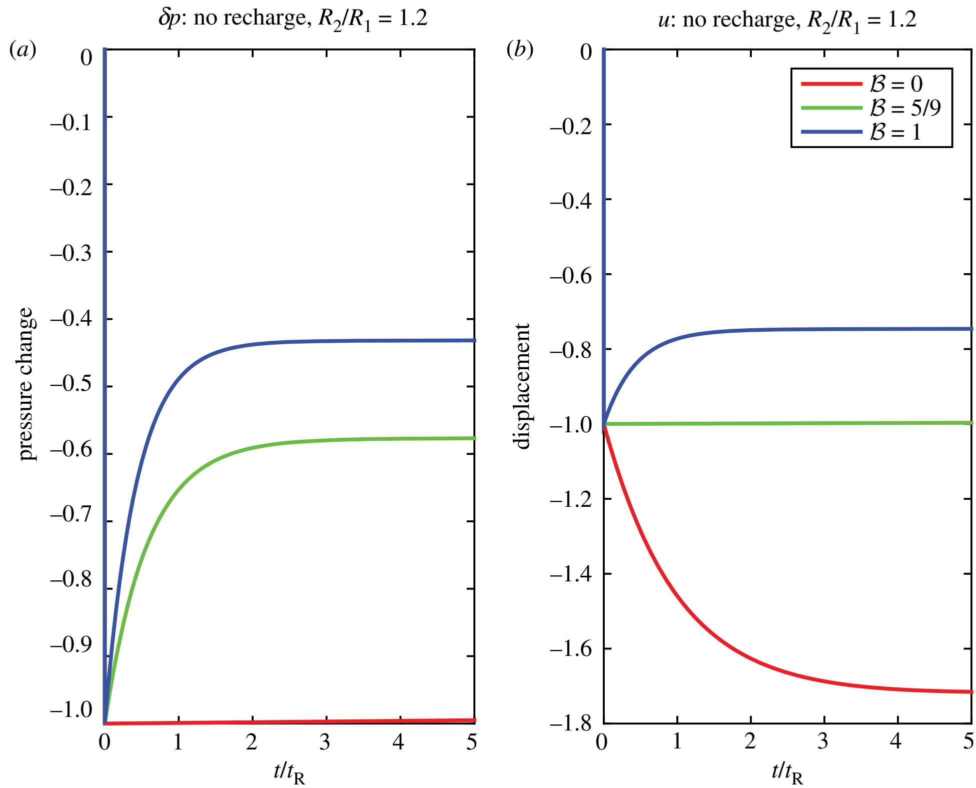

Figure 5. No-recharge limit. (*a*) Normalized chamber pressure; (*b*) normalized displacement in the elastic region. For infinitely compressible magma, the chamber pressure is constant following eruption and the co-eruption subsidence continues. For an incompressible magma, the chamber pressure partially recovers and there is partial re-inflation following the eruption, even though there is no flow into the chamber. For $\mathcal{B} = \frac{5}{9}$, there is no post-eruptive deformation even though the pressure is increasing. Here $\nu = 0.25$, $R_2/R_1 = 1.2$. After Segall [19].

Wikipedia in the Introduction. In particular, the ratio of the fully relaxed response ($t \to \infty$) to the instantaneous elastic response is given by

$$\frac{u(t \to \infty)}{u(t = 0)} = \frac{(R_2/R_1)^3}{1 + [3(1 - \nu)/(1 + \nu)]\mathcal{B}[(R_2/R_1)^3 - 1]}. \tag{2.7}$$

Whether the final subsidence exceeds the co-eruptive subsidence depends on whether the ratio in (2.7) is greater or less than 1. From (2.7), post-eruptive deflation occurs when $\mathcal{B} < (1 + \nu)/3(1 - \nu)$; for $\nu = \frac{1}{4}$ this ratio is $\frac{5}{9} \approx 0.56$. For larger values of $\mathcal{B}$ (relatively incompressible magmas), the final deflation is less than the immediate post-eruptive deflation; that is, the co-eruptive deflation partially recovers. Note also that for $\nu = 0.5$ and $\mathcal{B} = 1$, $u(t \to \infty) = u(t = 0)$; in this case both the magma and the surrounding are incompressible, and there is no change in volume as the viscoelastic shell relaxes.

The limiting behaviour is illustrated in figure 5. Note that in the no-recharge limit there is only one time constant. It depends only on t_R; without recharge, there is no dependence on τ.

Because this analysis is for a very idealized geometry of a spherical chamber with a spherical viscoelastic shell, it is reasonable to ask whether inflation without mass injection is general, i.e. whether it can occur for more realistic magma chamber geometries? I test this using FEM calculations in §3. Before that, I review the response of the spherical system with recharge.

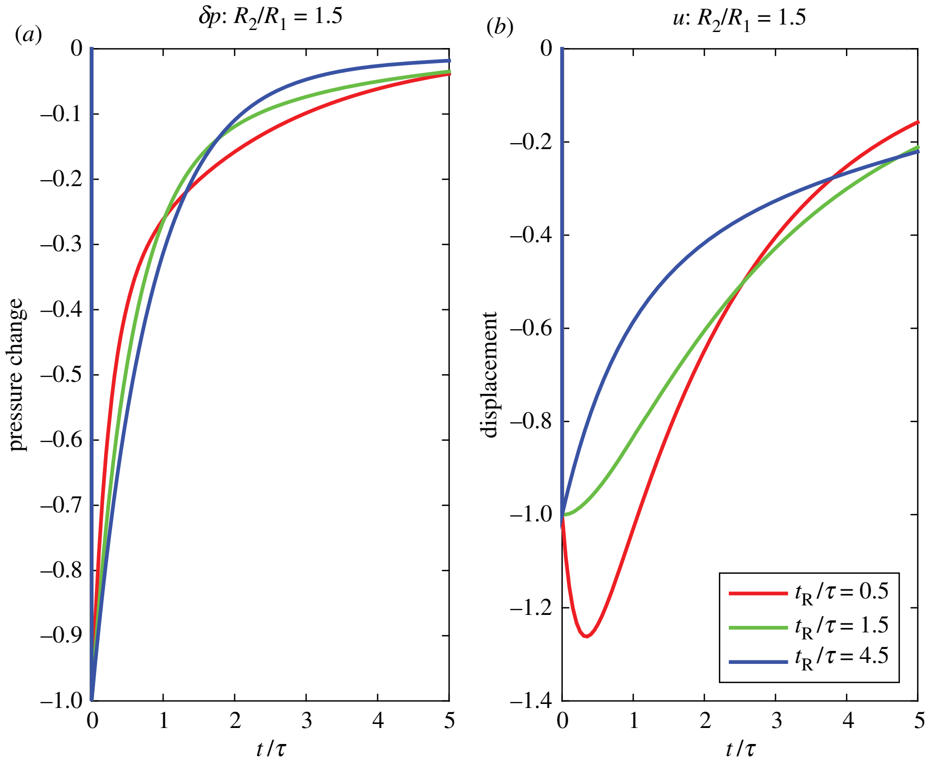

Figure 6. (*a*) Pressure and (*b*) displacement for $R_2/R_1 = 1.5$ and $\mathcal{B} = 0.2$. The *y*-axis scales are normalized by the co-eruptive pressure and displacement changes, respectively. After Segall [19].

(b) Response with recharge

It is interesting to determine whether the immediate response following an explosive eruption is inflationary or deflationary, something that would be easy to identify with field data. Segall [19] derived an expression for the boundary between the deflationary and inflationary fields. Assuming relatively low rate of pre-eruptive inflation such that $\Delta p_0/\delta p_0^+ \ll 1$, the boundary between inflating and deflating scenarios is given by

$$\frac{t_R}{\tau} = \left[\left(\frac{R_2}{R_1}\right)^3 - 1\right]\left[1 - \frac{3(1-\nu)}{(1+\nu)}\mathcal{B}\right]. \tag{2.8}$$

Examples are shown in figure 6, for relatively small $\mathcal{B}$; that is, a relatively compressible magma. For a given value of $\mathcal{B}$, we find that for large t_R/τ the response approaches the elastic limit, as expected, and the immediate response is inflationary. By contrast, for small t_R/τ rapid stress relaxation causes a deflation before recharge reverses the trend and causes inflation.

Figure 7 illustrates equation (2.8) graphically, separating fields in which the instantaneous post-eruptive response is inflationary versus deflationary as functions of t_R/τ and $\mathcal{B}$ for different ratios of outer to inner radii. For a given ratio R_2/R_1, any combination of t_R/τ and $\mathcal{B}$ above the line exhibits immediate post-eruptive inflation; $t_R/\tau = 0$ corresponds to the no-recharge limit. The predictions from this plot can be compared with the numerical results shown in figure 6. For $R_2/R_1 = 1.5$ (green curve) and $\mathcal{B} = 0.2$ the boundary between inflationary and deflationary responses occurs at $t_R/\tau = 1.5$. Figure 6 shows that for this ratio of t_R/τ the inflation rate indeed vanishes at $t = 0$, as predicted. Larger values of t_R/τ move into the inflationary field, while smaller values exhibit post-eruptive deflation, as illustrated in figure 6.

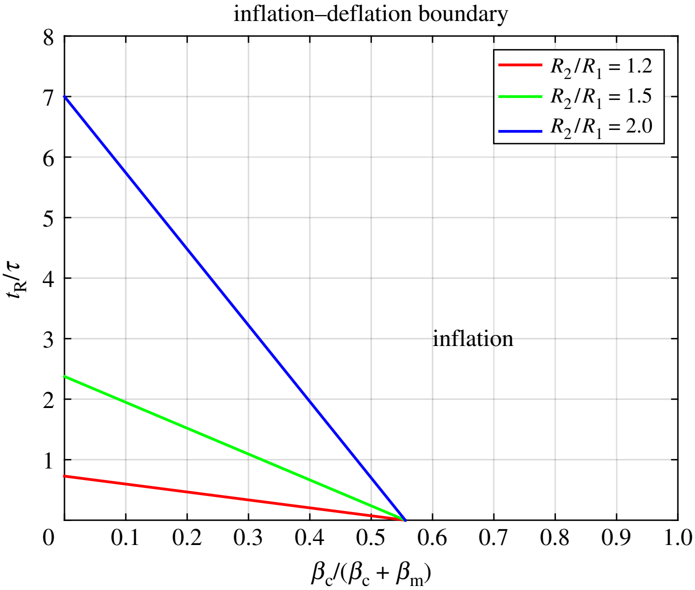

Figure 7. Boundary between instantaneous post-eruptive inflation and deflation for different values of R_2/R_1. Values to the right and above the line experience immediate post-eruptive inflation. The limit of $t_R/\tau = 0$ corresponds to the no-recharge limit. After Segall [19].

Given GPS time series it should be possible to constrain parameters of interest, including $\mathcal{B}$ and t_R/τ. In this approach, we leverage knowledge of the form of the pressure history, namely a step decrease in pressure during the eruption, to remove some ambiguity in the deconvolution problem discussed above. However, it must be recognized that this model is greatly simplified in assuming a single shell with spatially uniform viscosity. Furthermore, other processes can cause deviations from exponential decay in flux as described in §4. Finally, many magmatic systems exhibit transient, episodic inflation, indicating that other, currently poorly understood, processes are at play as discussed briefly in §5.

3. Viscoelastic effects with generalized chamber geometries

Because the analytical results in the previous section are so idealized, it is important to verify whether similar behaviour is observed with different chamber geometries. Motivated by the conceptual model of a magma chamber by Cashman *et al.* [15], as in figure 2, I consider a magma reservoir with an oblate spheroidal geometry. The viscoelastic aureole is also an ellipsoid but is offset so that the viscoelastic region is thicker on the bottom, perhaps representing a cumulate zone (figure 8). Calculations are performed using the finite-element code COMSOL. A pressure drop corresponding to a short-lived eruption is imposed at $t = 0$; following that, the mass of fluid within the chamber is held fixed, corresponding to the no-recharge limit discussed above.

As expected from the spherical case, for relatively incompressible magmas ($\mathcal{B} > 0.5$) there is partial re-inflation, even with no mass addition within the reservoir (figure 8*a*). Interestingly, for intermediate values of compressibility $\mathcal{B}$, the behaviour is non-monotonic. That is, there may be some post-eruptive deflation followed by re-inflation, with slight differences between the vertical and radial components. The reason for this is that stresses within the viscoelastic aureole relax at different rates in different locations. This is seen in figure 8*b*, which shows the maximum deviatoric stress after one relaxation time. The shear stresses above the reservoir have mostly relaxed, concentrating stress at the lateral edge of the chamber. It is worth emphasizing that the

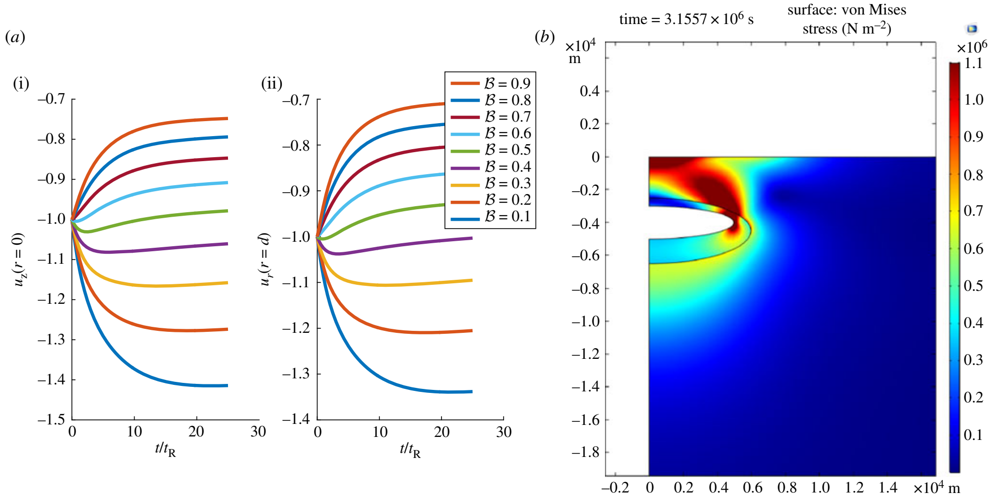

Figure 8. Deformation associated with an oblate magma chamber surrounded by a Maxwell viscoelastic aureole. (*a*)(i) Vertical displacement u_z evaluated at $z = 0, r = 0$; (ii) radial displacement u_r evaluated at $z = 0, r = d$ as a function of normalized time t/t_R. Here d is the chamber centroid depth and (in this figure) $t_R = \eta/\mu$ is the Maxwell relaxation time. Curves are drawn for different values of $\mathcal{B}$. Displacements are scaled by the co-eruptive deflation, that is, $u(t = 0) = -1$. (*b*) Radial–vertical section through the model. Colours show the maximum shear (von Mises) stress at $t\mu/\eta = 1$.

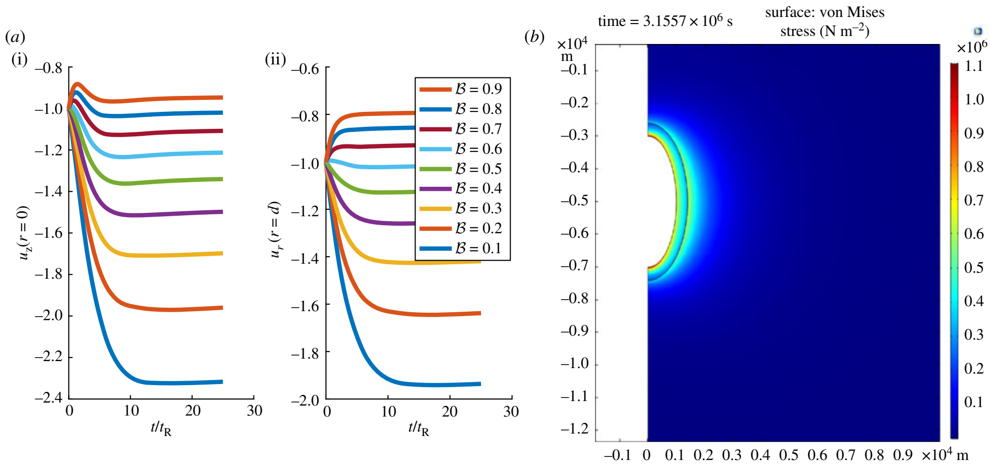

Figure 9. Deformation associated with a prolate magma chamber surrounded by a Maxwell viscoelastic aureole. (*a*)(i) Vertical displacement u_z evaluated at $z = 0, r = 0$; (ii) radial displacement u_r evaluated at $z = 0, r = d$ as a function of normalized time t/t_R. Here d is the chamber centroid depth and $t_R = \eta/\mu$ is the relaxation time. Curves are drawn for different values of $\mathcal{B}$. Displacements are scaled by the co-eruptive deflation, that is, $u(t = 0) = -1$. (*b*) Radial–vertical section through the model. Colours show the maximum shear (von Mises) stress at $t\mu/\eta = 1$.

non-monotonic surface deformation, including partial re-inflation, results from an instantaneous pressure drop and no mass flow into the magma chamber.

Next, I consider a prolate spheroid as illustrated in figure 9. As in the oblate geometry, for sufficiently large $\mathcal{B}$ there is partial re-inflation, even though the mass of magma is held constant. For the radial displacement at $z = 0, r = d$, this occurs for $\mathcal{B} > 0.6$ and is smaller in magnitude than in the oblate case, although it should be noted that the viscoelastic aureole is considerably thinner

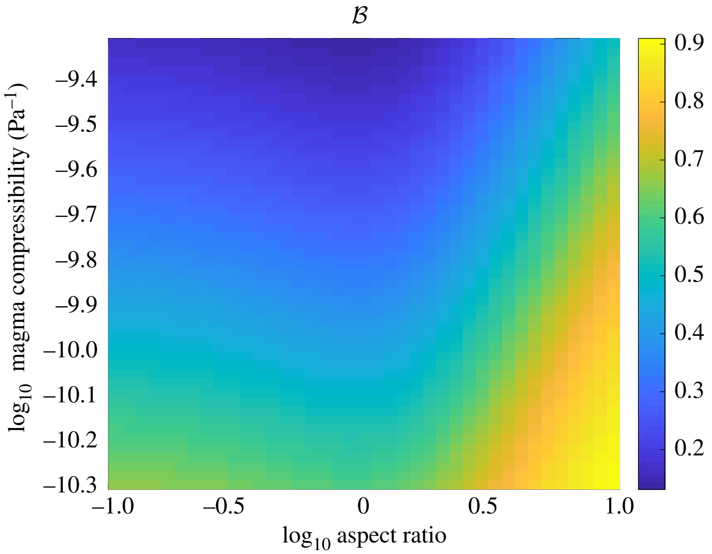

Figure 10. Values of $\mathcal{B} = \beta_c/(\beta_m + \beta_c)$ as a function of aspect ratio (horizontal/vertical) and magma compressibility β_m. Numerical calculations are for centroid depth of 1 km, volume equivalent to a sphere with radius 1 km and shear modulus of 10 GPa.

in this calculation. The vertical displacement directly above the chamber is more complex; for $\mathcal{B} > 0.6$ there is some inflation, followed by deflation. Again, the non-monotonicity is striking.

Whether or not post-eruptive inflation can occur without recharge depends critically on $\mathcal{B}$, which in turn depends on the relative compressibility of the magma and elastic chamber (equation (2.6)). The latter depends on crustal stiffness (shear modulus), and importantly the chamber shape and distance from the free surface; it is difficult to compute analytically. Figure 10 shows $\mathcal{B}$ as a function of magma compressibility and aspect ratio computed numerically following [27]. Comparing to figures 9 and 8 suggests that, especially for oblate chambers, relative degassed magmas could be sufficiently incompressible to cause post-eruptive inflation without mass influx.

4. Recharge with nonlinear magma rheology

The viscoelastic results discussed above show that surface deformation resulting from a rapid de-pressurization can have complex time dependence. In the simple analytical model for a spherical chamber and aureole, the response is the sum of two exponential decays. For sufficiently low viscosity, this can yield a short-term response, dominated by viscoelastic relaxation, and a longer-term response, dominated by time-dependent recharge. Such behaviour has been observed for example at Grímsvötn volcano in Iceland. Viscoelastic response, however, is not the only mechanism that could give rise to such behaviour. Reverso *et al.* [28] suggest that a second, deep magma chamber could give rise to the observed time dependence. Got *et al.* [29] argue for the effects of increasing damage around the chamber, although this would require a large and widespread decrease in elastic stiffness. Another possible mechanism is nonlinearity in recharge.

Consider recharge with power-law magma rheology: $\dot{\gamma} = c\tau^n$, where $\dot{\gamma}$ and τ are the shear strain rate and maximum shear stress, respectively, c is a constant, and n is the power-law exponent. For a vertical circular conduit with radius R, integration of the equilibrium equation in the z-direction yields $\sigma_{rz}(r) = (r/R)\sigma_{\text{wall}}$, where σ_{wall} is the shear stress acting on the conduit wall. Combining this with the above constitutive law to derive the velocity distribution, and then integrating to obtain the mass flux, yields

$$q_{\text{in}} = \frac{\rho_0 \pi c R^3}{n+3}\left(\frac{R}{2}\frac{\mathrm{d}p}{\mathrm{d}z}\right)^n. \tag{4.1}$$

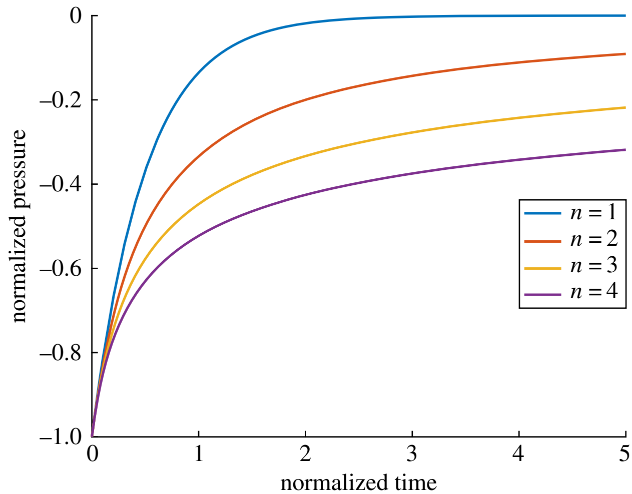

Figure 11. Pressure recovery with nonlinear rheology in an elastic Earth model. Time is normalized by $(p^{\infty})^{1-n}/\Omega^*$.

Thus, the governing ordinary differential equation for chamber pressure, combining (4.1) with mass conservation (1.2), is

$$\frac{\mathrm{d}p}{\mathrm{d}t} = \Omega^*(p^{\infty} - p)^n, \tag{4.2}$$

where Ω^* is a modified flux parameter appropriate for the nonlinear rheology. Taking the pressure gradient to be $(p^{\infty} - p)/L$, one obtains

$$\Omega^* = \frac{\pi c R^3}{(n+3)V_0(\beta_m + \beta_c)}\left(\frac{R}{2L}\right)^n. \tag{4.3}$$

Equation (4.2) can be integrated exactly to yield

$$\delta p(t) = \Delta p_0 - [(n-1)\Omega^* t + (\Delta p_0 - \delta p_0^+)^{1-n}]^{1/(1-n)}, \quad n \neq 1. \tag{4.4}$$

Results are shown in figure 11. For a Newtonian ($n = 1$) magma, the pressure recovery is exponential (equation (1.4)). For shear-thinning fluids ($n > 1$), the recharge starts rapidly but then slows with time as the pressure gradient declines. This behaviour is qualitatively similar to that observed at Grímsvötn volcano.

5. Future challenges

Future work will be required to address expected deformation signals from more complex multi-level models motivated by geologic and geophysical observations (e.g. [15]). In particular, it will be important to understand to what extent surface deformations are sensitive to processes below shallow crustal reservoirs. In many, if not most, cases volcanic inflation is not accompanied by sensible deflation associated with deeper sources. Yet, mass must be conserved between all sources and sinks. The absence of observable deflation may be because sources are too deep or distributed to produce clear deformation signals, or it may in part result from pressure-dependent compressibility of magmas (e.g. [30]). Nevertheless, being able to geodetically image magma source regions would be a significant step forward in our understanding of how magmatic systems work.

Simple models predict time-dependent pressurization of crustal magma chambers (e.g. equation (1.4)). Consideration of viscoelastic relaxation reveals the potential for more complex and even non-monotonic behaviour (figure 6). At the same time, many volcanoes exhibit transient, episodic inflation and, in some cases, these events are associated with increased flux of magma from mantle sources, as evidenced by increased CO_2 flux [31]. Are these episodic inflations caused by dykes depositing melt into crustal reservoirs? Or by nonlinear behaviour in long-lived conduits? The rate of influx, q_{in} in (1.2), is almost certainly not constant, even though this is sometimes assumed for mathematical convenience.

One approach that we can expect to gain prominence is the integration of independent datasets with geodetic data to provide tighter constraints on parameters of interest (e.g. [32]). Of course, such efforts face their own challenges: seismic tomography potentially provides information about magma chamber geometry; however seismic travel times or waveform fitting are generally interpreted in terms of three-dimensional distribution of elastic wave speeds; translating that information into melt volume fraction is challenging. Nevertheless, some studies have integrated petrologic and seismic data with satellite geodetic data to better constrain magmatic conditions (e.g. [33]). Kilbride *et al.* [34] combine InSAR observations of deflation with observations of atmospheric sulfur loading and thermodynamic models to better understand the nature of exsolved volatiles within magma reservoirs. Volcano-tectonic earthquakes represent brittle response of the crust to the same processes that cause measurable surface deformation, and thus should be amenable to joint analysis. For example, Segall *et al.* [35] used the model of Dieterich [36] to propose methods for jointly analysing deformation and seismicity data recorded during dyke injections. The limitations of volcano geodesy alone to constrain important properties of magma chambers suggests that integration with complementary datasets will grow in importance in coming years.

Data accessibility. No primary data were used in this paper.
Competing interests. I have no financial or other competing interests.
Funding. This work was supported by the U.S. National Science Foundation grant no. EAR-1358607.
Acknowledgements. I thank the editor and two anonymous reviewers.

References

1. Biggs J, Ebmeier S, Aspinall W, Lu Z, Pritchard M, Sparks R, Mather T. 2014 Global link between deformation and volcanic eruption quantified by satellite imagery. *Nat. Commun.* **5**, 3471. (doi:10.1038/ncomms4471)
2. Mogi K. 1958 Relations between the eruptions of various volcanoes and the deformations of the ground surfaces around them. *Bull. Earthq. Res. Inst. Univ. Tokyo* **36**, 111–123.
3. Segall P. 2010 *Earthquake and volcano deformation*. Princeton, NJ: Princeton University Press.
4. McTigue DF. 1987 Elastic stress and deformation near a finite spherical magma body—resolution of the point-source paradox. *J. Geophys. Res.* **92**, 12 931–12 940. (doi:10.1029/JB092iB12p12931)
5. Yang XM, Davis PM, Dieterich JH. 1988 Deformation from inflation of a dipping finite prolate spheroid in an elastic half-space as a model for volcanic stressing. *J. Geophys. Res. Planets* **93**, 4249–4257. (doi:10.1029/JB093iB05p04249)
6. Cervelli PF. 2013 Analytical expressions for deformation from an arbitrarily oriented spheroid in a half-space. In *AGU Fall Meeting Abstracts*. See https://ui.adsabs.harvard.edu/?#abs/2013AGUFM.V44C..06C
7. Fialko Y, Khazan Y, Simons M. 2001 Deformation due to a pressurized horizontal circular crack in an elastic half-space, with applications to volcano geodesy. *Geophys. J. Int.* **146**, 181–190. (doi:10.1046/j.1365-246X.2001.00452.x)
8. Dzurisin D. 2003 A comprehensive approach to monitoring volcano deformation as a window on the eruption cycle. *Rev. Geophys.* **41**, 1001. (doi:10.1029/2001rg000107)
9. Berrino G, Corrado G, Luongo G, Toro B. 1984 Ground deformation and gravity changes accompanying the 1982 Pozzuoli uplift. *Bull. Volcanol.* **47**, 187–200. (doi:10.1007/BF01961548)
10. Rymer H, Williams-Jones G. 2000 Volcanic eruption prediction: magma chamber physics from gravity and deformation measurements. *Geophys. Res. Lett.* **27**, 2389–2392. (doi:10.1029/1999GL011293)
11. Battaglia M, Segall P, Roberts C. 2003 The mechanics of unrest at Long Valley caldera, California. 2. Constraining the nature of the source using geodetic and micro-gravity data. *J. Volcanol. Geotherm. Res.* **127**, 219–245. (doi:10.1016/S0377-0273(03)00171-9)

12. Trasatti E, Giunchi C, Bonafede M. 2003 Effects of topography and rheological layering on ground deformation in volcanic regions. *J. Volcanol. Geotherm. Res.* **122**, 89–110. (doi:10.1016/S0377-0273(02)00473-0)
13. Hautmann S, Gottsmann J, Sparks RSJ, Mattioli GS, Sacks IS, Strutt MH. 2010 Effect of mechanical heterogeneity in arc crust on volcano deformation with application to Soufrière Hills volcano, Montserrat, West Indies. *J. Geophys. Res. Solid Earth* **115**, B09203. (doi:10.1029/2009JB006909)
14. Hickey J, Gottsmann J, Mothes P, Odbert H, Prutkin I, Vajda P. 2017 The ups and downs of volcanic unrest: insights from integrated geodesy and numerical modelling. In *Advances in Volcanology*. Berlin, Germany: Springer. (doi:10.1007/11157_2017_13)
15. Cashman KV, Sparks RSJ, Blundy JD. 2017 Vertically extensive and unstable magmatic systems: a unified view of igneous processes. *Science* **355**, eaag3055. (doi:10.1126/science.aag3055)
16. Mastin LG, Roeloffs E, Beeler NM, Quick JE. 2008 Constraints on the size, overpressure, and volatile content of the Mount St. Helens magma system from geodetic and dome-growth measurements during the 2004–2006+ eruption. In *A volcano rekindled: the renewed eruption of Mount St. Helens, 2004–2006* (eds DR Sherrod, WE Scott, PH Stauffer), ch. 22, pp. 461–488. U.S. Geological Survey Professional Paper 1750.
17. Sturkell E *et al.* 2006 Volcano geodesy and magma dynamics in Iceland. *J. Volcanol. Geotherm. Res.* **150**, 14–34. (doi:10.1016/j.jvolgeores.2005.07.010)
18. Dragoni M, Magnanensi C. 1989 Displacement and stress produced by a pressurized, spherical magma chamber, surrounded by a viscoelastic shell. *Phys. Earth Planet. Inter.* **56**, 316–328. (doi:10.1016/0031-9201(89)90166-0)
19. Segall P. 2016 Repressurization following eruption from a magma chamber with a viscoelastic aureole. *J. Geophys. Res. Solid Earth* **121**, 8501–8522. (doi:10.1002/2016JB013597)
20. Bonafede M, Dragoni M, Quareni F. 1986 Displacement and stress fields produced by a centre of dilation and by a pressure source in a viscoelastic half-space: application to the study of ground deformation and seismic activity at Campi Flegrei, Italy. *Geophys. J. Int.* **87**, 455–485. (doi:10.1111/j.1365-246X.1986.tb06632.x)
21. Newman A, Dixon T, Ofoegbu G, Dixon J. 2001 Geodetic and seismic constraints on recent activity at Long Valley caldera, California: evidence for viscoelastic rheology. *J. Volcanol. Geotherm. Res.* **105**, 183–206. (doi:10.1016/S0377-0273(00)00255-9)
22. Newman AV, Dixon TH, Gourmelen N. 2006 A four-dimensional viscoelastic deformation model for Long Valley caldera, California, between 1995 and 2000. *J. Volcanol. Geotherm. Res.* **150**, 244–269. (doi:10.1016/j.jvolgeores.2005.07.017)
23. Del Negro C, Currenti G, Scandura D. 2009 Temperature-dependent viscoelastic modeling of ground deformation: application to Etna volcano during the 1993–1997 inflation period. *Phys. Earth Planet. Inter.* **172**, 299–309. (doi:10.1016/j.pepi.2008.10.019)
24. Masterlark T, Haney M, Dickinson H, Fournier T, Searcy C. 2010 Rheologic and structural controls on the deformation of Okmok volcano, Alaska: FEMs, InSAR, and ambient noise tomography. *J. Geophys. Res. Solid Earth* **115**, B02409. (doi:10.1029/2009JB006324)
25. Yamasaki T, Kobayashi T, Wright TJ, Fukahata Y. 2018 Viscoelastic crustal deformation by magmatic intrusion: a case study in the Kutcharo caldera, eastern Hokkaido, Japan. *J. Volcanol. Geotherm. Res.* **349**, 128–145. (doi:10.1016/j.jvolgeores.2017.10.011)
26. Currenti G. 2018 Viscoelastic modeling of deformation and gravity changes induced by pressurized magmatic sources. *J. Volcanol. Geotherm. Res.* **356**, 264–277. (doi:10.1016/j.jvolgeores.2018.03.020)
27. Anderson K, Segall P. 2011 Physics-based models of ground deformation and extrusion rate at effusively erupting volcanoes. *J. Geophys. Res. Solid Earth* **116** (B7), B07204. (doi:10.1029/2010JB007939)
28. Reverso T, Vandemeulebrouck J, Jouanne F, Pinel V, Villemin T, Sturkell E, Bascou P. 2014 A two-magma chamber model as a source of deformation at Grímsvötn volcano, Iceland. *J. Geophys. Res. Solid Earth* **119**, 4666–4683. (doi:10.1002/2013JB010569)
29. Got J-L, Carrier A, Marsan D, Jouanne F, Vogfjörd K, Villemin T. 2017 An analysis of the nonlinear magma–edifice coupling at Grímsvötn volcano (Iceland). *J. Geophys. Res. Solid Earth* **122**, 826–843. (doi:10.1002/2016jb012905)

30. Rivalta E, Segall P. 2008 Magma compressibility and the missing source for some dike intrusions. *Geophys. Res. Lett.* **35**, 1251. (doi:10.1029/2007GL032521)
31. Poland M, Miklius A, Montgomery-Brown EK. 2015 Magma supply, storage, and transport at shield-stage. In *Characteristics of Hawaiian volcanoes* (eds M Poland, T Takahashi, CM Landowski), p. 179. U.S. Geological Survey Professional Paper 1802.
32. Anderson K, Segall P. 2013 Bayesian inversion of data from effusive volcanic eruptions using physics-based models: application to Mount St. Helens 2004–2008. *J. Geophys. Res.* **118**, 2017–2037. (doi:10.1002/jgrb.50169)
33. Field L, Blundy J, Brooker R, Wright T, Yirgu G. 2012 Magma storage conditions beneath Dabbahu volcano (Ethiopia) constrained by petrology, seismicity and satellite geodesy. *Bull. Volcanol.* **74**, 981–1004. (doi:10.1007/s00445-012-0580-6)
34. Kilbride BM, Edmonds M, Biggs J. 2016 Observing eruptions of gas-rich compressible magmas from space. *Nat. Commun.* **7**, 13744. (doi:10.1038/ncomms13744)
35. Segall P, Llenos A, Yun S-H, Bradley A, Syracuse E. 2013 Time-dependent dike propagation from joint inversion of seismicity and deformation data. *J. Geophys. Res. Solid Earth* **118**, 5785–5804. (doi:10.1002/2013JB010251)
36. Dieterich J. 1994 A constitutive law for rate of earthquake production and its application to earthquake clustering. *J. Geophys. Res.* **99**, 2601–2618. (doi:10.1029/93JB02581)